Water Practice & Technology

IWA PUBLISHING

Water Practice & Technology Vol 18 No 9, 2136 doi: 10.2166/wpt.2023.132

Adsorption of aniline from aqueous solutions onto a nanoporous material adsorbent: isotherms, kinetics, and mass transfer mechanisms

Nisreen S. Ali[a], Hasan Sh. Majdi[b], Talib M. Albayati[c,*] and Dheyaa J. Jasim[d,e]

[a] Materials Engineering Department, College of Engineering, Mustansiriyah University, Baghdad, Iraq
[b] Department of Chemical Engineering and Petroleum Industries, Al-Mustaqbal University College, Babylon 51001, Iraq
[c] Department of Chemical Engineering, University of Technology-Iraq, 52 Alsinaa St., P.O. Box 35010, Baghdad, Iraq
[d] Department of Petroleum Engineering, Al-Amarah University College, Maysan, Iraq
[e] General Company for Food Products, Ministry of Industry and Minerals, Baghdad 10011, Iraq
*Corresponding author. E-mail: talib.m.naieff@uotechnology.edu.iq

TMA, 0000-0001-5619-7760

ABSTRACT

MCM-48, which is particulate and nanoporous, was formulated to actively remove aniline (AN) (i.e., benzenamine) from wastewater. MCM-48 was characterized by several methods. It was found that the MCM-48 was highly active in adsorbing aniline from wastewater. The Langmuir, Freundlich, and Temkin isotherms were employed to evaluate the adsorption equilibrium. At 100 and 94 mg g^{-1}, the maximum theoretical and experimental absorption of aniline, respectively, fit with a Type I Langmuir isotherm. The Langmuir model was optimal in comparison to the Freundlich model for the adsorption of AN onto the mesoporous material MCM-48. The results of these kinetics adsorption models were investigated using model kinetics that employed both pseudo-first- and pseudo-second-order models as well as models utilized intraparticle diffusion. The kinetics adsorption models demonstrated that the absorption was rapid and most closely agreed with the pseudo-first-order model. The kinetic studies and the adsorption isotherms revealed the presence of both physical adsorption and chemisorption. The potential adsorption mechanisms include the following: (1) hydrogen bonding, (2) π-π interactions, (3) electrostatic interaction, and (4) hydrophobic interactions. The solution's pH, ionic strength, and ambient temperature also played essential roles in the adsorption.

Key words: benzenamine, kinetics adsorption, mass transfer, mechanism adsorption, mesoporous material, wastewater treatment

HIGHLIGHTS

- The mesoporous silica MCM-48 was very successful to remove aniline.
- A maximum aniline adsorption 94 mg/g was achieved on MCM48 adsorbent.
- MCM-48 was found very active for the removal of aniline compounds from wastewater.
- Aniline adsorption mechanism is a chemisorption and physical adsorption process.
- The MCM-48 was regenerated and reused efficiently in a batch adsorption.

1. INTRODUCTION

Industries, including those in the food, pharmaceutical, petrochemical, chemical, pulp, electronics, and paper sectors, all create enormous amounts of waste discharges with considerable potential for recycling and remediation (Alardhi *et al.* 2020; Ali *et al.* 2023; Humadi *et al.* 2023; Muslim *et al.* 2023). In the paint, plastic, pesticide, dye, and intermediate industries of the chemical industries, aniline (C_6H_7N) is widely used (Ahmad & Tan 2004; Ali *et al.* 2022a; Jabbar *et al.* 2022; Abbood *et al.* 2023). Many serious environmental problems have been caused by wastewater containing aniline because of its carcinogenic properties and high toxicity. It is usually remediated by both physical and chemical techniques, including precipitation coagulation, filtration, ion exchange, ozonation, membrane, advanced oxidation processes, and adsorption (Goncharuk *et al.* 2002; Hirakawa *et al.* 2007). In addition, various types of adsorption methods have been employed to remove organic and inorganic contaminants from wastewater, with a variety of materials selected as the adsorbent.

Adsorption can be defined as a phenomenon where solutes or gases are sorbed by either liquid or solid surfaces as part of a mechanism for mass transmission. The molecules or atoms on the solid surface are adsorbed due to uneven forces because they have an abundance of surface energy (Hu & Xu 2020; Cabooter *et al.* 2021). Regenerating used adsorbent materials is costly and time-consuming (Al-Bastaki 2004). Therefore, research has sought novel adsorbents to eliminate contamination in wastewater (Morent *et al.* 2006), including silicate (Levec & Pintar 2007), mesoporous materials (Bhargava *et al.* 2007), and zeolites, either modified or unmodified (Ko *et al.* 2007). Zeolites act as an adsorbent material because they have the ability either to adsorb particular compounds or to prohibit such adsorption; they manage this as a result of the physical characteristics of the molecules (e.g., size, shape, and polarity). In addition, research on organ clays has demonstrated their ability to adsorb organic molecules from water.

For some applications, MCM-48 has produced good results (Al-Nayili *et al.* 2022). Current research has focused on mesoporous materials (i.e., MCM-41, MCM-48, and SBA-15) because of their potential use as catalysts, catalyst supports, and absorbents as well as in drug delivery, photocatalysis, and desulfurization (Atiyah *et al.* 2022a, 2022b). These materials have characteristic properties that include a volume of specific pores that can be as large as 1.2 cm^3/g, with surface areas of 1,000–1,500 m^2/g and pore sizes that are narrow, have high thermal stability, and are non-cytotoxic (Narita *et al.* 1985). MCM-48 and other mesoporous silica-based substances have been generated for various functions – as adsorbents, carriers of catalysts, and effective drug delivery systems (Taralkar *et al.* 2008). These mesoporous materials have substantial thermal stability, extensive surface areas, a porous morphology, and contain surfaces that are extremely reactive to silanol groups (Shaban *et al.* 2017; Pajchel & Kolodziejski 2018).

The present research sought to study how to optimally remove aniline (C_6H_7N) from wastewater with MCM-48 as the adsorbent. The effectiveness of this process was evaluated using adsorption kinetics and isotherms. Furthermore, a batch adsorption process was employed to investigate the mass transfer mechanism of aniline wastewater onto the MCM-48 surface adsorbent. Both desorption and regeneration kinetics were evaluated to determine the utility of the adsorbent and whether it could withstand being reused without impacting its performance.

2. EXPERIMENTAL DESIGN

2.1. Materials

This study used the surfactant cetyl trimethyl ammonium bromide (CTAB), with a purity greater than 98%; the silica source tetraethyl orthosilicate (TEOS), with a purity greater than 98%; hydrochloric acid (HCl); and sodium hydroxide (NaOH). All chemicals were purchased from Sigma Aldrich Chemical Company and used without modification.

2.2. MCM-48 preparation

MCM–48 was synthesized using the method delineated in Doyle & Hodnett (2003), Doyle *et al.* (2006) and Nejat *et al.* (2015). First, deionized water (90 g) was mixed with CTAB (10 g). Next, the solution was agitated at high speed and at 35 °C for 40 min, after which NaOH (1 g) was added. The mixture was stirred for 60 min at 35 °C before 11 cm^3 of TEOS was added, after which the mixture continued to be stirred under the same conditions for an additional 30 min. The mixture was put into an autoclave for 24 h at a constant temperature (150 °C). Then, the prepared MCM-48 was cooled for 1 h, filtered, and rinsed with distilled H_2O prior to being allowed to dry at room temperature. Next, the MCM-48 underwent calcination for 6 h. The temperature was increased to 650 °C at a ramp rate of 2 °C/min.

2.3. Characterization

2.3.1. EDAX and SEM analyses

An energy-dispersive X-ray analysis (EDAX) spectrometer was employed to determine the chemical composition during the experiments. It was paired with scanning electron microscopy (SEM; JEOL JSM-5600 LV) to make it more powerful.

2.3.2. X-ray diffraction (XRD)

A small-angle diffractometer (MiniFlex, Rigaku) was used to apply XRD to determine the phase identification of a crystalline material and unit cell dimensions. The instrument was used in ambient settings using Cu K radiation

($\lambda = 1.5406$ Å). At 40 kV and 30 mA, the 10 s step time was used to record data from an X-ray tube with a step size of 0.01 and a step time of 0.5–80. The unit cell was found using $n\lambda = 2d\sin\theta$, and the d-spacing was found using $a_o = 2d100/\sqrt{3}$.

2.3.3. BET and PSD analysis

A pore analyzer (Micrometrics ASAP 2020) used N2 physisorption to measure the adsorption and desorption of nitrogen at a temperature of –196 °C. A degassing procedure was carried out for 3 h on all specimens in the degas adsorption analyzer port at 350 °C and under vacuum ($p < 10^{-5}$ mbar). Calculating the BET-specific surface area led to a relative pressure ranging from 0.05 to 0.25. To determine the pore size distributions, thermodynamics and the Barrett–Joyner–Halenda (BJH) method were used, based on the isotherm desorption branch. The total pore volume was found by observing the amount of liquid N2 adsorbed at the relative pressure ($P/P_0 = 0.995$), based on the adsorption branch of the N2 isotherm. The thickness of the pore walls (t_W) was assessed based on the unit cell parameter (a_o) and pore size diameter (d_P). Brunauer–Emmett–Teller (BET) analysis (4 V/A) was employed to determine the average mesopore sizes for each specimen based on the nitrogen sorption data.

2.3.4. FT-IR analysis

A Fourier-transform infrared (FT-IR) spectrometer (NICOLET 380) was used to measure the infrared spectra of the solid samples. They were found to range between 4,000 and 400 cm^{-1} in areas with a resolution of 4 cm^{-1} at room temperature.

2.4. Experiments of batch adsorption

Batch adsorption tests were conducted to evaluate the aniline isotherms of adsorption onto the adsorbents at 25 °C. Stock solutions of aniline were prepared by dissolving 0.2 g in 1 L of distilled H_2O. Next, a calibration curve was generated based on 10 concentrations (i.e., ranging from 0 to 0.2 g/L) using a UV-spectrometer (model HP 8453) calibrated to 25 °C. The value of λ_{max} was 280 nm. To compare the final absorbance with the beginning absorbance, calibration was necessary. Fifteen concentrations (i.e., 0.001–0.06 g/L) of the solutions described above were prepared in 100-mL conical flasks. Using 0.01 g MCM-48, 100 mL of each solution was added, followed by stirring at 150 rpm for 1 h at room temperature (25 °C). This allowed the mixtures to combine totally with the mesoporous material MCM-48. After the adsorption procedure, equal amounts of the solutions were centrifuged for 5 min at 3,500 rpm using a centrifuge (Hermle Z 200 A). Aniline's $\%R$ can be expressed using the following equation (Khader *et al.* 2023):

$$\%R = \frac{C_o - C_e}{C_o} \times 100\% \tag{1}$$

Equation (2) was used to determine the adsorption amount (q_e) (Muslim *et al.* 2022):

$$q_e = \frac{V(C_o - C_e)}{m} \tag{2}$$

where q_e (mg/g) indicates the amount of aniline to be absorbed; V (L) indicates the volume of the solution of aniline; C_0 (mg/L) and C_e (mg/L) are the aniline concentrations at the start and at equilibrium in the liquid phase, respectively; and m (g) indicates the absorbent mass (Al-Khodor & Albayati 2023).

2.5. Adsorption isotherm model

Three isotherm models (i.e., Langmuir, Freundlich, and Temkin) were evaluated to determine which agreed optimally with the aniline adsorption data. A linearization equation based on Langmuir's model (Han *et al.* 2004) is as follows:

$$\frac{C_{eq}}{q_e} = \frac{1}{q_m} C_{eq} + \frac{1}{K_L\, q_m} \tag{3}$$

where q_m (mg/g) indicates the adsorption capacity associated with the Langmuir constant, K_L (L/mg) indicates the adsorption energy constant, the constants q_m and K_L relate to a linear form of Equation (3), represented by the slope of $\frac{C_{eq}}{q_e}$ versus C_{eq}.

The dimensionless constant or separation factor that is the equilibrium parameter (R_L) can be expressed as (Webber & Chakkravorti 1974):

$$R_L = \frac{1}{1 + K_L C} \tag{4}$$

The value of R_L indicates four possible conditions of the isotherm: (1) favorable ($R_L < 1$), (2) unfavorable ($R_L > 1$), (3) linear ($R_L = 1$), or (4) irreversible ($R_L = 0$) (Chen *et al.* 2010).

Equation (5) presents the Freundlich in linear form (Freundlich 1906):

$$\ln q_e = \ln K_f + \frac{1}{n} \ln C_{eq} \tag{5}$$

The Freundlich constants n and K_f represent the sorbent's capacity and the adsorption intensity, respectively. To evaluate n and K_f, the slope and intercept of the line associated with ln q_e are compared with ln C_e.

The linear expression for the Temkin isotherm model is expressed in the following equation (Temkin & Pyzhev 1940):

$$q_e = \frac{RT}{b_T} \ln K_T + \frac{RT}{b_T} \ln C_e \tag{6}$$

where K_T represents the equilibrium binding constant (L/g), (equivalent to the extreme binding energy), b_T represents the Temkin isotherm constant (related to heat adsorption at 8.314 J/mol K), and T represents the absolute temperature (°K). The isotherm constants b_T and K_T are found by plotting ln q_e versus ln C_e.

2.6. Adsorption kinetics

To study the adsorption kinetics of adsorption on the adsorbent material MCM-48, three models were employed (i.e., pseudo-first-order, pseudo-second-order, and intraparticle diffusion) because they are the most widely applied models. Equation (7) expresses the integrated pseudo-first-order model (Lagergren 1898):

$$\text{Log}\ (q_e - q_t) = \text{Log} q_e - k_1 t \tag{7}$$

where q_e represents the amount adsorbed (mg/g) at equilibrium, while q_t represents the amount adsorbed at time t; k_1 represents the constant in the pseudo-first-order rate (h^{-1}), which is determined using the slope of the line plotted by Log ($q_e - q_t$) versus t.

The adsorbed aniline quantity at equilibrium time t is shown by q_e and q_t, respectively. The pseudo-first-order adsorption equilibrium rate has a constant, k_1.

Equation (8) evaluates the pseudo-second-order model (Qiang *et al.* 2013):

$$\frac{t}{q_t} = \frac{1}{k_2 qe^2} + \frac{1}{qe} t \tag{8}$$

where k_2 is the pseudo-second-order rate constant (g/mg min), which is determined by plotting t/q_t versus t.

In contrast, the equation associated with the intraparticle diffusion model is shown in the following equation (Al-Bayati 2014):

$$q_t = k_{id} t^{0.5} + C \tag{9}$$

where k_{id} (mg g $\text{min}^{0.5}$) indicates the constant for the intraparticle diffusion rate, while C indicates the constant related to intraparticle diffusion. If a line can be drawn when plotting q_t versus $t^{0.5}$, it signifies that the adsorption process is limited to intraparticle mass transfer. However, if a number of linear plots can be drawn using the same data, it demonstrates that the adsorption process has been greatly influenced by the multiple phases associated with the aforementioned stages (Ali *et al.* 2022b). The values of C indicate the boundary layer thickness, with lower values of the intercept signifying that the boundary layer has less of an effect (Albayati & Doyle 2014a).

2.7. Mechanism and mass transfer

In Equation (9), the intraparticle diffusion model – the Weber and Morris (WM) model – is used to investigate the surface mass transfer mechanism in relation to the adsorbent pores (Lagergren 1898). The theoretical basis is Fick's second law of diffusion (Fauzia *et al.* 2018). Most of the time, the pore-based diffusion of the particle can control the adsorption process. The Bangham and Burt (BB) paradigm, shown in Equation (10), can be employed (Albayati & Doyle 2013). Whether or not the surface adsorption is regulated by the pore diffusion is irrelevant when using the BB model:

$$\log \log\left[\frac{C_i}{C_i - q_t\, m}\right] = \log\left[\frac{K_b m}{2.303V}\right] + \alpha \log(t) \tag{10}$$

where v and m represent the adsorbent mass and the volume of the solution, respectively. Furthermore, K_b and α represent constants in the BB equation.

2.8. Reuse of the adsorbent

The MCM-48 adsorbent under investigation had been exhausted in order to study how well it would regenerate. After the aniline solution was absorbed onto the MCM-48, the solution was filtered, and the adsorbent material laden with aniline was well rinsed in water until all of the aniline was removed from the solution. Then, the aniline was dried in a vacuum at 60 °C overnight. The materials underwent a few adsorption–desorption cycles to evaluate the MCM-48's ability to regenerate as well as its resilience.

3. RESULTS AND DISCUSSION

3.1. Characterization of the adsorbent

Both SEM and EDAX were employed to characterize the prepared MCM-48. The SEM photographs are displayed in Figure 1(a), with a magnification of 1,000×. Figure 1(b) displays peaks showing that the zeolite was predominantly composed of C, O, and Si, based on the average weight % values provided by the EDAX. Using the EDAX data, graphs were created for a number of locations on the SEM photos.

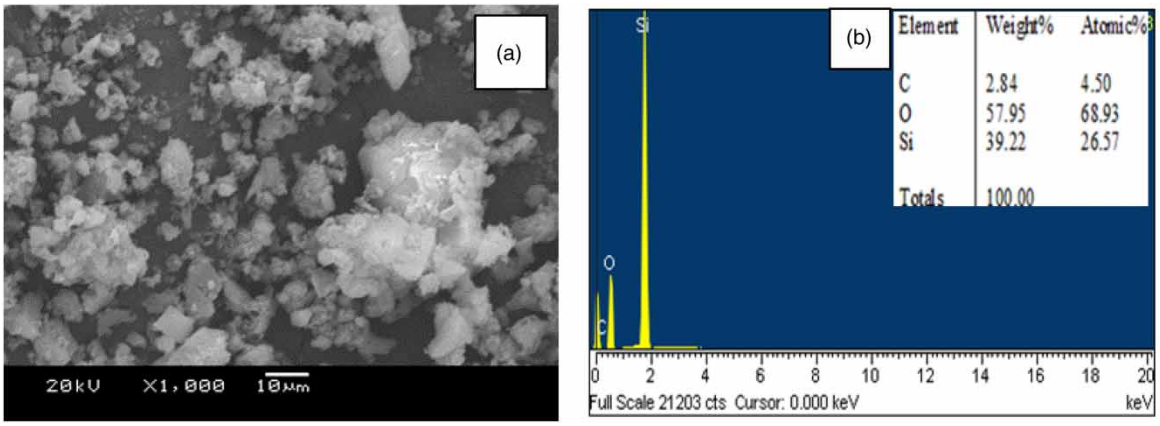

Figure 1 | (a) SEM picture of MCM-48 at a 1,000× magnification. (b) A typical MCM-48 EDAX picture.

Figure 2(a) presents the small-angle XRD patterns of the MCM-48, showing a clear-cut mesostructured diffraction peak at approximately 2θ of 0.9°. The XRD results also displays two peaks at (2 1 1) and (2 2 0). Two reflection peaks that occurred at less than 3° as well as a series of weaker reflection peaks between 3.5° and 5.5° indicate the Ia3d cubic structure. The peaks found in this study agree with those in the literature (Han *et al.* 2004). Additionally, Table 1 reveals MCM-48's periodic and ordered structure. According to Figure 2(b), both type H1 hysteresis loops and Type IV isotherms were present in MCM-48's N2 adsorption isotherms. The sharp adsorption line along with similar desorption branches signify small pore sizes. In isotherms, a capillary condensation process is characterized by its sharpness and height, and typically, the pore size of mesoporous

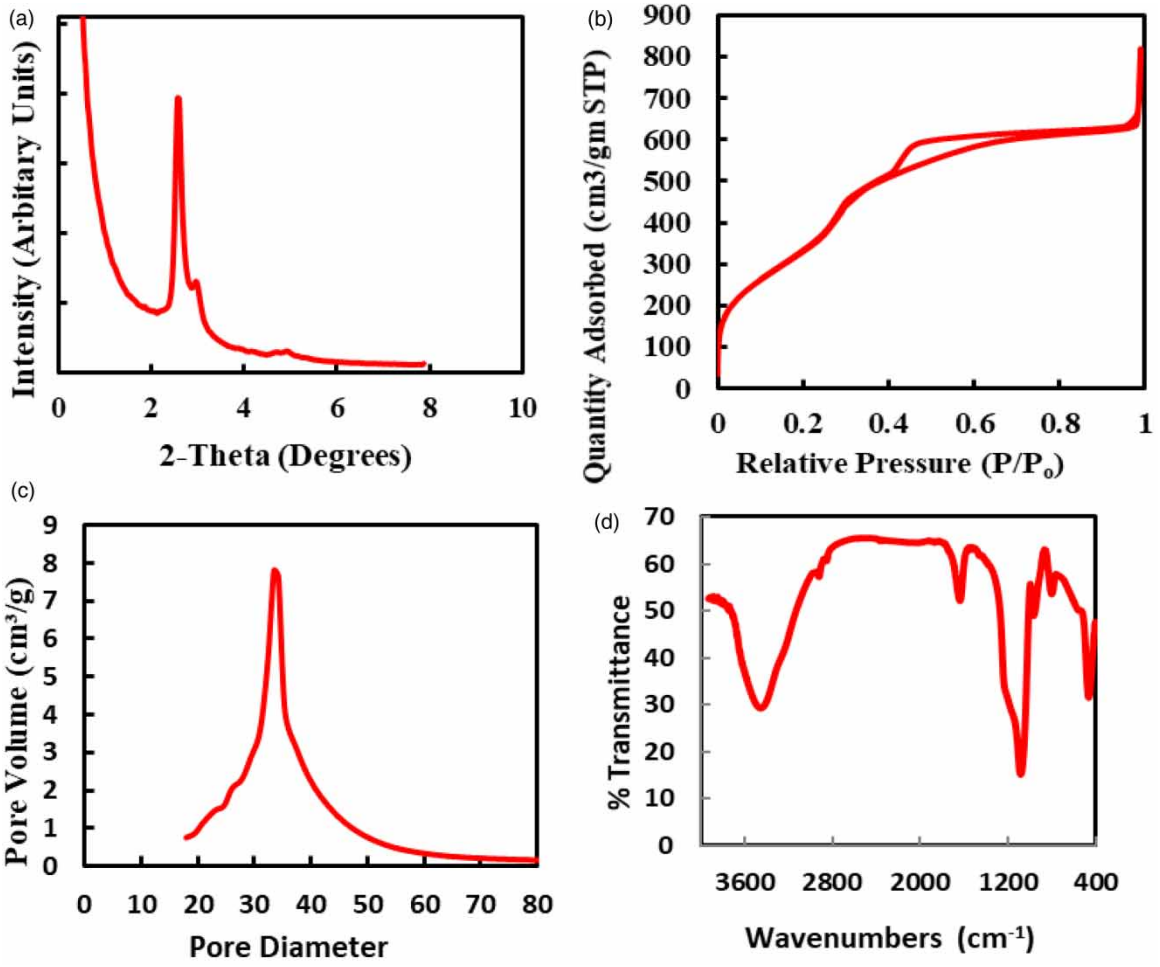

Figure 2 | MCM-48: (a) XRD pattern, (b) isotherms of nitrogen adsorption–desorption, (c) BJH PSD, and (d) FT-IR spectra.

Table 1 | MCM-48's physicochemical characteristics

Sample	S_{BET} (m^2/g)	V_P (cm^3/g)	$V_{\mu P}$ (cm^3/g)	D_P (nm)	a_o (nm)	t_{wall} (nm)
MCM-48	1,400	1.3	0.4	3	3.5	0.6

molecular sieves falls between 0.05 and 0.25 relative pressure (P/P_0). Therefore, the MCM-48 reveals a Type IV isotherm, as shown in Figure 2(b). Table 1 describes the sample's pore size, specific surface area, wall thickness, and pore volume along with other morphological aspects that have been found in nitrogen adsorption studies. The MCM-48 pore size distribution (PSD) is shown in Figure 2(c). The PSD of the CTAB: NaOH: TEOS was centered and broad at 34 Å. After the synthesis of MCM-48, a greater number of mesopores were found, thereby supporting the conclusion that the MCM-48 had a fairly regular organization and pore size dispersion (Albayati & Doyle 2014b). The FT-IR spectra of MCM-48 that occurred at 1,082, 964, 799, and 460 cm^{-1} showed characteristic Si–O–Si bands, as seen in Figure 2(d). For both Si–OH and Si–O–Si, the stretching vibrations relate to the absorption band that occurred at about 960 cm^{-1}. The wide band near 3,463 cm^{-1} was produced by the surface OH groups and their strong H_2 bonding interactions. Additionally, the distortion modes of the OH bonds of the adsorbed water resulted in the band close to 1,637 cm^{-1} (Saad *et al.* 2007).

3.2. Aniline adsorption

3.2.1. Effect of the agitation speed

To study the adsorption of the contaminated solution, the contact time and solution concentration were held constant while the agitation velocity was altered from 0 to 200 rpm. More contaminants were removed when the

agitation velocity increased from 0 to 150 rpm, after which the removal did not change. Hence, if the agitation velocity ranges from 150 to 200 rpm, the cationic sites in the pores of the MCM-48 will be readily available for absorption. Thus, 150 rpm was determined to be the optimal agitation speed for further studies (Temkin & Pyzhev 1940).

3.2.2. Effect of the pH

To effectively eliminate aniline from wastewater, the solution's pH must facilitate protonation and adsorption. The primary factor in optimal efficiency is the adsorbent's surface charge, and it is regulated by the pH (Saad *et al.* 2007). Figure 3 illustrates the fact that the removal efficiency of dye ions by the adsorbent slowly decreased when the solution's pH rose from 1 to 6; however, this decrease occurred more quickly when the pH level reached 5. High pH levels are less conducive to the effective absorption of dye ions because of the electrostatic repulsion effect, as protons compete with the dye ions for binding sites on the adsorbent's surface. However, a lower pH creates a decrease in the proton concentration, thereby increasing the number of binding sites and accelerating the absorption of dye.

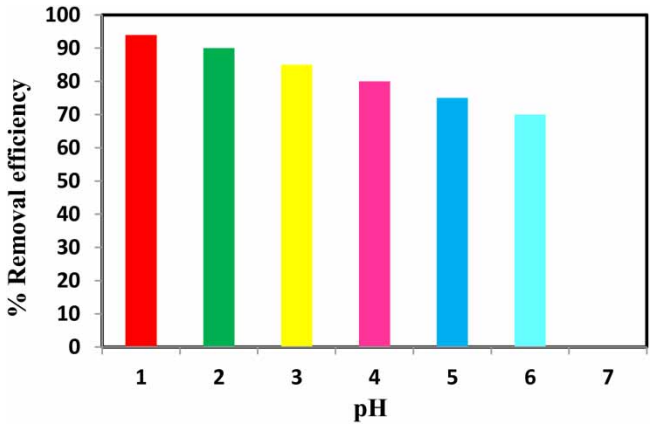

Figure 3 | Effect of pH on removal of aniline dye at contact time = 60 min, concentrations = 4 mg/L, temperature = 25 °C, adsorbents dose = 0.01 g, and shaking rotary speed = 150 rpm.

3.2.3. Concentration effect

Using the initial concentration function C_0, Figure 4 depicts the % removal of aniline estimated by Equation (1). Approximately 85% of the aniline (initially 4 mg dm^{-3}) was eliminated from the solution. With a constant mass of MCM-48, the % removal of aniline declined as the concentration rose because there was less of the concentrated solution to absorb additional dye ions. As the maximum absorption of the MCM-48 pores approaches, less material can be adsorbed (Lagergren 1898).

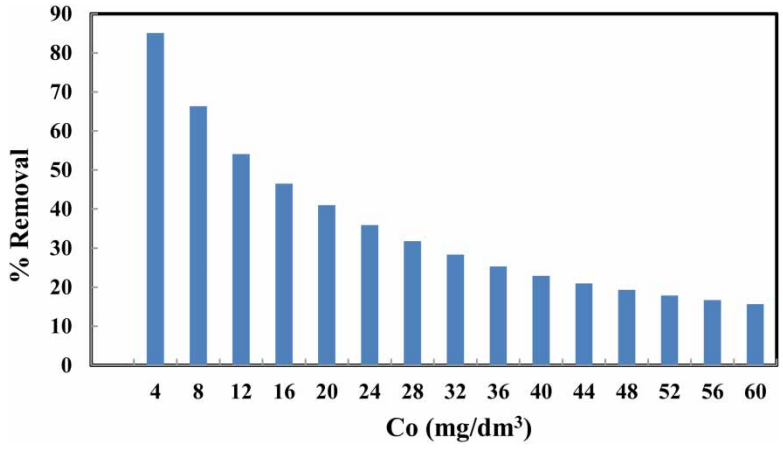

Figure 4 | Initial aniline concentration impact on removal efficiency at contact time = 60 min and MCM-48 dosage = 0.01 g.

3.3. Adsorption isotherm

The adsorption isotherms of the aniline compound are depicted in Figure 5(a), where C_e signifies the adsorbate concentration in the solution at equilibrium, and, as the name suggests, q_e corresponds to the amount of the adsorbate that was adsorbed for every gram of the MCM-48. The MCM-48 was both effective and efficient in removing aniline within solutions of various concentrations. Another factor that must be considered is the initial adsorbate concentration because it needs to overcome all ion and molecule mass transfer resistances that might occur between the solid and liquid phases (Qiang *et al.* 2013). In the present study, the initial solution concentration ranged between 4 and 60 mg/L, while the MCM-48 level remained constant at 0.01 g/100 mL. As shown in Figure 5(a), an increase in the equilibrium adsorption capacity led to an increase in the initial aniline concentration as well. The equilibrium adsorption of the aniline rose from 34 to 94 mg/g as the aniline aqueous solution concentration rose from 4 to 60 mg/L as a result of an excessive number of AN molecule with contaminated solutes competing for a small number of binding sites on the surface of the adsorbent. Figure 5(a) shows that the cationic surfactants, including MCM-48, were able to adsorb a large amount of aniline. As illustrated in Figure 2(d), silanol groups (Si–OH) were also noteworthy sites of adsorption that were extant in this substance along with the cationic sites that were provided by a cationic template. Thus, the number of sorption sites is a major factor in the adsorption of aniline on MCM-48, which initially contained a great number of empty surface sites for adsorption. It is also possible that over time a strong attractive force was created between the aniline molecules and the sorbent. Toward the end of the process, saturation will also make it problematic to fill any open surface sites (Al-Bayati 2014).

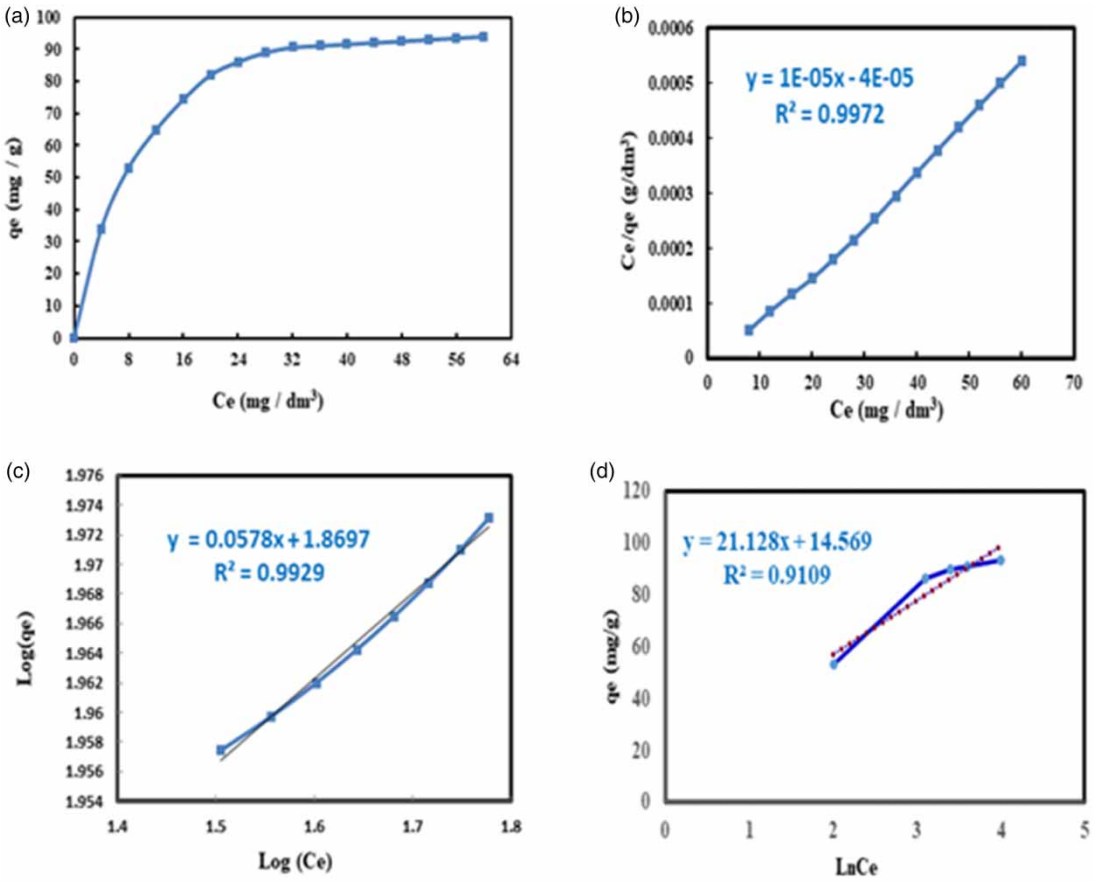

Figure 5 | (a) Aniline adsorption equilibrium onto MCM-48, (b) Langmuir isotherm (c) Freundlich, and (d) Temkin isotherms.

The adsorption isotherm profiles for aniline fit the Langmuir Type I adsorption model; the quantity adsorbed rose gradually until it reached values in the 34–94 mg/g range (Ali *et al.* 2022b). Adsorption isotherms have been studied in order to model adsorption behavior. Therefore, Figure 5(a)–5(c) displays the Langmuir, Freundlich, and Temkin isotherm models in order to evaluate the process of aniline adsorption. Table 2 provides the

Table 2 | Aniline adsorption on MCM-48 according to the Langmuir, Freundlich, and Temkin models

	Langmuir constants				Freundlich constants			Temkin constants		
Adsorbate	Q_{max} (mg/g)	K_L (dm^3 mg^{-1})	R^2	R_L	1/n	K_F	R^2	b_T	Ln K_T	R^2
Aniline	100	0.25	0.9972	0.45	0.0578	74.079	0.9929	117.7	0.047	0.9109

regression coefficients, showing R^2 values of 0.99. Such a high correlation coefficient indicates that there is a strong agreement between the parameters. Figure 5(b) employs the Langmuir model to produce a straight line, indicating Type I adsorption of the aniline. When adsorbed, aniline may produce monolayers as large as 100 mg/g, based on the constant q_{max}. Additionally, aniline has an adsorption energy constant, K_L, of 0.25 dm^3/mg. Table 2 lists the equilibrium parameter (R_L) values based on the Langmuir isotherm model, showing that all R_L values were greater than 0 but less than 1, which signifies that the Langmuir isotherm is favorable (Chen *et al.* 2010).

As shown in Figure 5(c), the data were also matched to the Freundlich equation, with Table 2 specifying the constants of regression. As stated above, the correlation coefficient values validate the Langmuir equation as an extremely close fit, making it a better model than either the Freundlich or the Temkin to describe aniline adsorption on mesoporous materials. Furthermore, aniline is highly adsorbable, as shown by it having 1/n values that are less than 1 (Albayati & Doyle 2014a). The final model (i.e., Temkin) is exhibited in Figure 5(d), with any relevant adsorption parameters listed in Table 2.

3.4. Adsorption kinetics

Figure 6(a) reveals the contact time required for the aniline solution to adsorb onto the MCM-48 and attain equilibrium, which took less than 20 min. Therefore, to saturate the MCM-48 adsorbent, only a short contact time was

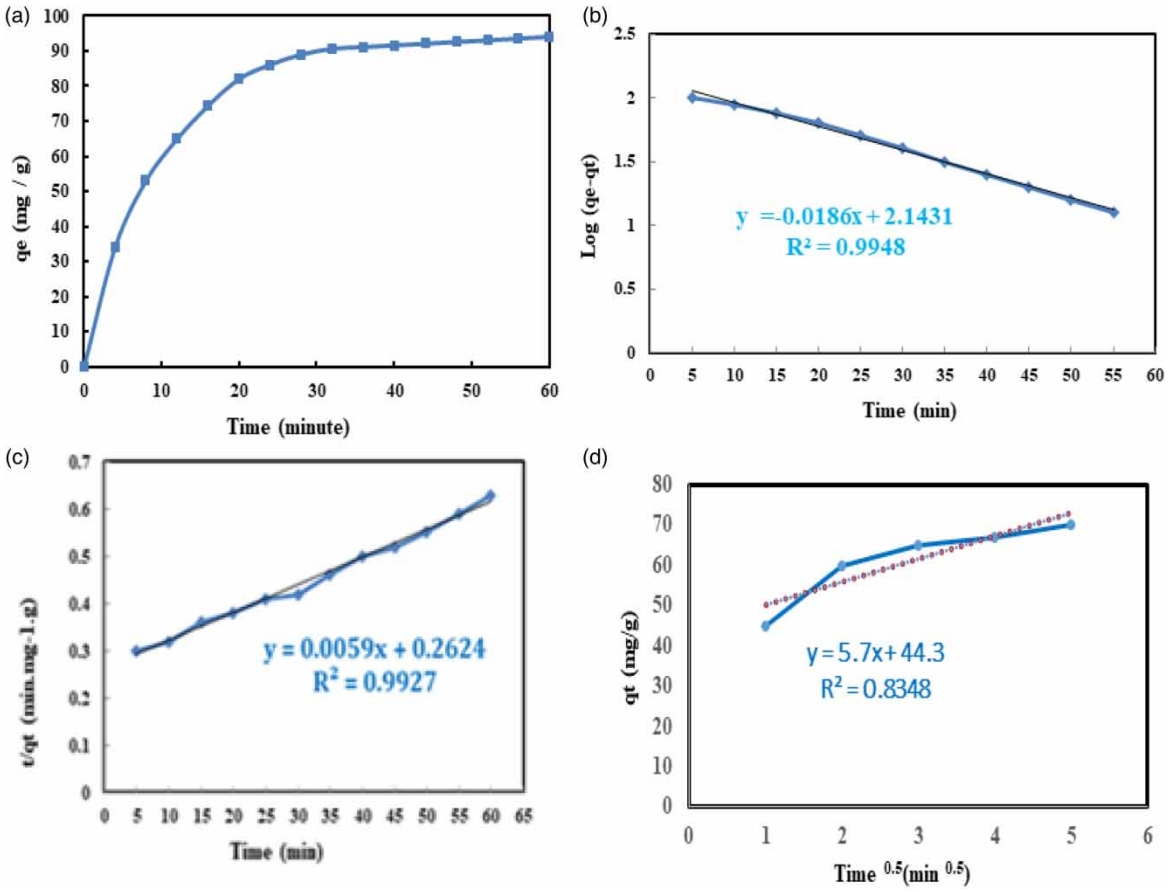

Figure 6 | (a) Aniline kinetics adsorption onto MCM-48, (b) pseudo-first order, (c) pseudo-second order, and (d) intraparticle diffusion model.

required. The higher cationic surfactant concentrations along with their high availability in the pores of the adsorbent greatly enhanced the adsorption capacity, which is significant because the time needed to reach equilibrium is one of the primary considerations when creating an efficient wastewater treatment system. Thus, the adsorption was allowed to continue for 1 h during all of the experiments (Khadim *et al.* 2022).

The rate of aniline adsorption is a key factor in its effectiveness. Both pseudo-first- and pseudo-second-order model (Kadhum *et al.* 2022) as well as intraparticle diffusion model were employed to elucidate the kinetics of AN adsorption, which can be seen in Figure 6(b)–6(d), respectively. The kinetic model variables are displayed in Table 3, where R^2 represents the correlation coefficient. Table 3 demonstrates that the theoretical values (q_e) from the pseudo-first-order kinetic model provided significantly dissimilar values than those found in the experiment (q_e exp.). Therefore, this adsorption system can be well described by the pseudo-first-order kinetic model, as shown in Figure 6(b). In contrast, the results presented in Table 3 show identical theoretical and experimental values (i.e., q_e cal. and q_e exp.) for the pseudo-second-order kinetic model. The coefficients' R^2 values approached 1, providing additional confirmation for describing the results by using the pseudo-second-order equation. As far as the adsorption mechanism is concerned, the pseudo-first-order hypothesis appears to be robust, especially as the regression coefficients are so close to 1 (0.9948) (Kadhum *et al.* 2021).

Table 3 | Constants of aniline kinetics adsorption on MCM-48 according to the pseudo-first order, second-order, and intraparticle diffusion model

		Pseudo-first order constants			Pseudo-second-order constants			Intraparticle diffusion constants	
Adsorbates	**q_e exp. (mg/g)**	**q_e cal. (mg/g)**	**K_1 (g/mg min)**	**R^2**	**q_e cal. (mg/g)**	**K_2 (g/mg min)**	**R^2**	**K_{id} (mg/g min$^{0.5}$)**	**R^2**
Aniline	94	139	0.0186	0.9948	169	$1.3266*10^{-4}$	0.9927	5.7	0.83

As presented in Figure 6(d), the experimental results were compared to the intraparticle diffusion model using Equation (9) to understand the mechanisms and rate-controlling processes that had occurred. The calculations of k_{id} that used the slope of the second stage line are displayed in Table 3, which lists a k_{id} value of 5.7 mg/g min$^{0.5}$ with a determination coefficient (R^2) of 0.83. The appearance of the horizontal dotted line in Figure 6(d) indicates that the AN ion in the third region underwent an extremely slow uptake due to the equilibrium adsorption (Ali *et al.* 2022c).

3.5. Adsorption mechanism

The structure of the adsorbate and adsorbent must be revealed in order to fully comprehend the adsorption mechanism process (see Figure 7). Aniline is organic and is a primary aromatic amine comprised of an amino group connected to a benzene ring. Of all mesoporous materials, MCM-48 is the most commonly used as a molecular sieve, with some unique characteristics. Despite its amorphous silica wall, MCM-48 is consistently mesoporous, with a long-range organized structure. MCM-48 is primarily composed of silanol groups. The adsorption mechanism that allows aniline to adsorb onto MCM-48 can be discovered by looking at several factors: (1) the structure of aniline, (2) the structure of MCM-48, and (3) experimental results of kinetic, FT-IR and EDX analyses.

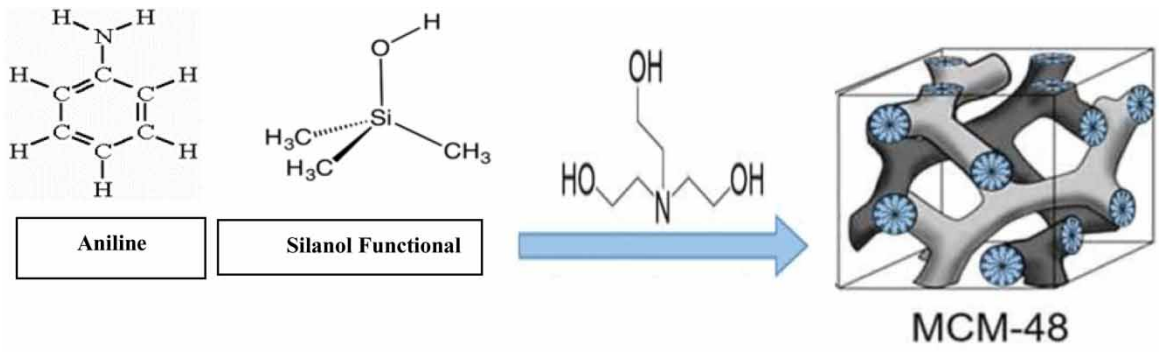

Figure 7 | Mechanism adsorption of MG onto MCM-48 adsorbent.

FT-IR showed that a clear-cut adsorption band of a –C = C– group diminished in intensity and also moved from 1,681 to 1,600 cm^{-1} due to the π–π interactions between the aniline and the –C = C– at the MCM-48's surface. In contrast, the intensity of the band of –OH groups rose and only showed a small shift from 3,330 to 3,335; this was due to the hydrogen bond that formed between the $-N(CH_3)_2$ group of the aniline molecules and the –OH group on the surface of the MCM-48. The carboxylic acid showed a band of C = O stretching vibrations that rose only a small amount in intensity as a result of the electrostatic attraction between the cationic $^{+}N(CH_3)_3^{+}$ group of MG molecules and the negatively charged COOH group on the MCM-48's surface. As stated above, the adsorption mechanism is both a chemisorption and physical adsorption process. Thus, there is adequate validation of aniline adsorption onto the MCM-48 surface due to a variety of mechanisms (e.g., electrostatic interaction, hydrogen bonding, and π–π interactions) (Amari *et al.* 2023).

3.6. Mass transfer models

This study presents the initial stage in analyzing the mass transfer of surface adsorption to predict the properties of MCM-48 adsorbents and surface adsorption. Table 4 shows the mass transfer models used (i.e., WM and BB) to evaluate the surface adsorption of dye molecules onto the adsorbent (Alorabi & Azizi 2023).

Table 4 | The surface adsorption process' associated characteristics from two mass transfer models

Intraparticle diffusion			Bangham and Burt		
I	K_p (mg/g $min^{0.5}$(	R^2	K_b (mL/g L)	α	R^2
44.3	5.7	0.83	0.0128	0.0434	0.9421

3.7. Adsorbent reuse

Desorption investigations were conducted to determine whether the MCM-48 could be reused after the adsorbates were removed. The experiments demonstrated that the aniline was efficiently and effectively desorbed (efficiency greater than 90%) into DI (deionized water) in only one cycle. Future work could research more about the particular mechanisms of desorption, such as the effects of adsorbate loading, solution concentration, temperature, etc. (Al-Jaaf *et al.* 2022). The results of regenerating and recycling the MCM-48 are shown in Figure 8, which indicates that the removal efficiency of the aniline changed only slightly, from 85 to 73% after five regeneration cycles. Therefore, MCM-48 can be easily reused and regenerated efficiently.

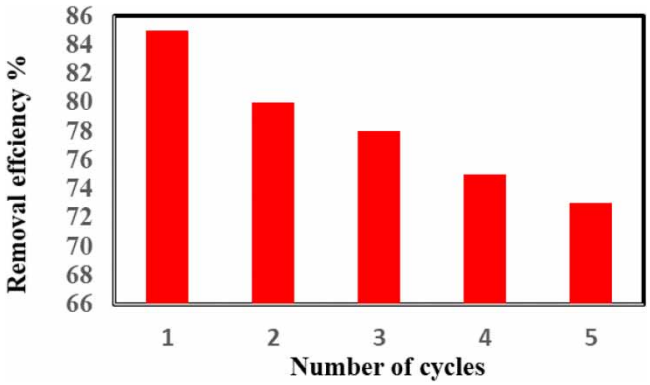

Figure 8 | The reusability of MCM-48 in batch experiment.

3.8. Comparative study

MCM-48 is compared with other adsorbents in Table 5, providing information about MCM-48's effectiveness as an adsorbent that might be able to increase aniline adsorption by adding other materials. Used without modification, the adsorption capability of MCM-48 was 94 mg/g for aniline. However, if a functional group was added to the MCM-48's surface, its adsorption capacity should increase. Overall, MCM-48 is an optimal adsorbent for aniline dye removal due to its large surface area that can reach 1,400 m^2/g (see Table 5).

Table 5 | Adsorption capacities of aniline by various adsorbents

No.	Adsorbents	Adsorption Capacity Q_{max} (mg/g)	References
1	AC	40.65	Liu *et al.* (2015)
2	ACS ACS/GO	78.13 136.98	Yi *et al.* (2020)
3	PS-HQ-HCP PS-CA-HCP PS-rE-HCP	210.9 167.4 160.9	Wang *et al.* (2023)
4	SBA-15	163.7	Koyuncu & Kul (2019)
5	NAC3	125.3	Chen *et al.* (2017)
6	MCM-48	94	This work

4. CONCLUSIONS

MCM-48, a mesoporous material, was able to effectively adsorb aniline from an aqueous solution and is thereby recommended for such use. The R^2 values of 0.99 demonstrated that aniline molecules fit with Type I Langmuir adsorption. Because the Langmuir adsorption isotherm best fits the experimental data, it can be assumed that the experiment showed a homogeneous surface with monolayer adsorption. The Langmuir isotherm calculated the theoretical adsorption capacity to be 100 mg/g and the experimental maximal adsorption capacity to be 94 mg/g. Therefore, this pseudo-first-order model can predict the adsorption dynamics of this system. Additionally, the adsorption isotherms and kinetics models demonstrate that both chemical and physical adsorption occurred within this adsorption mechanism.

ACKNOWLEDGEMENTS

The authors would like to express their gratitude to the Chemical Engineering Department at the University of Technology in Iraq, the Materials Engineering Department at Mustansiriyah University's College of Engineering in Baghdad, Iraq, and the Department of Chemical and Petroleum Industries Engineering at Al-Mustaqbal University College in Babylon, Iraq.

AUTHOR CONTRIBUTIONS

N. S. and T. M. conceptualized the whole article, developed the methodology, investigated the process, rendered support in data curation, and wrote the original draft; I. K. wrote the review and edited the article, and supervised the work; D. J. conceptualized the whole article, supervised the work, wrote the review and edited the article.

FUNDING

Not applicable.

DATA AVAILABILITY STATEMENT

All relevant data are included in the paper or its Supplementary Information.

CONFLICT OF INTEREST

The authors declare there is no conflict.

REFERENCES

Abbood, N. S., Ali, N. S., Khader, E. H., Majdi, H. S., Albayati, T. M. & Cata Saady, N. M. 2023 Photocatalytic degradation of cefotaxime pharmaceutical compounds onto a modified nanocatalyst. *Research on Chemical Intermediates*. https://doi.org/10.1007/s11164-022-04879-3.

Ahmad, A. L. & Tan, K. Y. 2004 Reverse osmosis of binary organic solute mixtures in the presence of strong solute-membrane affinity. *Desalination* **165**, 193–199.

Alardhi, S. M., Alrubaye, J. M. & Albayati, T. M. 2020 Removal of methyl green dye from simulated waste water using hollow fiber ultrafiltration membrane. In: *2nd International Scientific Conference of Al-Ayen University (ISCAU-2020), IOP Conf. Series: Materials Science and Engineering*, Vol. 928, p. 052020. doi:10.1088/1757-899X/928/5/052020.

Al-Bastaki, M. N. 2004 Performance of advanced methods for treatment of wastewater: UV/TiO_2, RO and UF. *Chemical Engineering and Processing* **43**, 935–940.

Al-Bayati, T. M. 2014 Removal of aniline and nitro-substituted aniline from wastewater by particulate nanoporous MCM-48. *Particulate Science and Technology: An International Journal* **32**(6), 616–623. doi:10.1080/02726351.2014.948973.

Albayati, T. M. & Doyle, A. M. 2013 Shape-selective adsorption of substituted aniline pollutants from wastewater. *Adsorption Science & Technology* **31**(5), 459–468. https://doi.org/10.1260/0263-6174.31.5.459.

Albayati, T. M. & Doyle, A. M. 2014a Purification of aniline and nitrossubistituted aniline contaminants from aqueous solution using beta zeolite. *Chemistry: Bulgarian Journal of Science Education* **23**(1), 105–114.

Albayati, T. M. & Doyle, A. M. 2014b SBA-15 Supported bimetallic catalysts for enhancement isomers production during n-heptane decomposition. *International Journal of Chemical Reactor Engineering* **12**(1), 345–354. doi:10.1515/ijcre-2013-0120.

Ali, N. S., Kalash, K. R., Ahmed, A. N. & Albayati, T. M. 2022a Performance of a solar photocatalysis reactor as pretreatment for wastewater via UV, UV/TiO_2, and UV/H_2O_2 to control membrane fouling. *Scientific Reports* **12**, 16782. https://doi.org/10.1038/s41598-022-20984-0.

Ali, N. S., Alismaeel, Z. T., Sh, H., Majdi, H. G., Salih, M. A., Abdulrahman, N. M., Saady, C. & Albayati, T. M. 2022b Modification of SBA-15 mesoporous silica as an active heterogeneous catalyst for the hydroisomerization and hydrocracking of n-heptane. *Heliyon* **8**, e09737. https://doi.org/10.1016/j.heliyon.2022.e09737.

Ali, N. S., Jabbar, N. M., Alardhi, S. M., Majdi, H. S. & Albayati, T. M. 2022c Adsorption of methyl violet dye onto a prepared bio-adsorbent from date seeds: Isotherm, kinetics, and thermodynamic studies. *Heliyon* **8**, e10276. https://doi.org/10.1016/j.heliyon.2022.e10276.

Ali, N. S., Harharah, H. N., Salih, I. K., Cata Saady, N. M., Zendehboudi, S. & Albayati, T. M. 2023 Applying MCM-48 mesoporous material, equilibrium, isotherm, and mechanism for the effective adsorption of 4-nitroaniline from wastewater. *Scientific Reports* **13**, 9837. https://doi.org/10.1038/s41598-023-37090-4.

Al-Jaaf, H. J., Ali, N. S., Alardhi, S. M. & Albayati, T. M. 2022 Implementing eggplant peels as an efficient bio-adsorbent for treatment of oily domestic wastewater. *Desalination and Water Treatment* **245**, 226–237. doi:10.5004/dwt.2022.27986.

Al-Khodor, Y. A. A. & Albayati, T. M. 2023 Real heavy crude oil desulfurization onto nanoporous activated carbon implementing batch adsorption process: Equilibrium, kinetics, and thermodynamic studies. *Chemistry Africa* https://doi.org/10.1007/s42250-022-00482-6.

Al-Nayili, A., Majdi, H. S., Albayati, T. M. & Cata Saady, N. M. 2022 Formic acid dehydrogenation using noble-metal nanoheterogeneous catalysts: Towards sustainable hydrogen-based energy. *Catalysts* **12**(3), 324. https://doi.org/10.3390/catal12030324.

Alorabi, A. Q. & Azizi, M. 2023 Effective removal of methyl green from aqueous environment using activated residual dodonaea viscosa: Equilibrium, isotherm, and mechanism studies. *Environmental Pollutants and Bioavailability* **35**(1), 2168761. doi:10.1080/26395940.2023.2168761.

Amari, A., Alawamleh, H. S. K., Isam, M., Maktoof, M. A. J., Osman, H., Panneerselvam, B. & Thomas, M. 2023 Thermodynamic investigation and study of kinetics and mass transfer mechanisms of oily wastewater adsorption on UIO-66–$MnFe_2O_4$ as a metal–organic framework (MOF). *Sustainability* **15**, 2488. https://doi.org/10.3390/su15032488.

Atiyah, N. A., Albayati, T. M. & Atiya, M. A. 2022a Functionalization of mesoporous MCM-41 for the delivery of curcumin as an anti-inflammatory therapy. *Advanced Powder Technology* **33**, 103417. https://doi.org/10.1016/j.apt.2021.103417.

Atiyah, N. A., Albayati, T. M. & Atiya, M. A. 2022b Interaction behavior of curcumin encapsulated onto functionalized SBA-15 as an efficient carrier and release in drug delivery. *Journal of Molecular Structure* **1260**, 132879. https://doi.org/10.1016/j.molstruc.2022.132879.

Bhargava, S. K., Tardio, J., Jani, H., Akolekar, D. D., Foeger, K. & Hoang, M. 2007 Catalytic wet-air oxidation of industrial waste streams. *Catalysis Surveys from Asia* **11**, 70–86.

Cabooter, D., Song, H., Makey, D., Sadriaj, D., Dittmann, M., Stoll, D. & Desmet, G. 2021 Measurement and modelling of the intra-particle diffusion and b-term in reversed-phase liquid chromatography. *Journal of Chromatography A* **1637**, 461852. https://doi.org/10.1016/j.chroma.2020.461852.

Chen, M., Chen, Y. & Diao, G. W. 2010 Adsorption kinetics and thermodynamics of methylene blue onto p-tert-Butyl-calix [4, 6, 8] arena-bonded silica Gel. *Journal of Chemical & Engineering Data* **55**, 5109–5116.

Chen, C. Y., Geng, X. H. & Huang, W. L. 2017 Adsorption of 4-chlorophenol and aniline by nanosized activated carbons. *Chemical Engineering Journal* **327**, 941–952.

Doyle, A. M. & Hodnett, B. K. 2003 Synthesis of 2-cyanoethyl-modified MCM-48 stable to surfactant removal by solvent extraction: Influence of organic modifier, base and surfactant. *Microporous and Mesoporous Materials* **58**, 255–261.

Doyle, A. M., Ahmed, E. & Hodnett, B. K. 2006 The evolution of phases during the synthesis of the organically modified catalyst support MCM-48. *Catalysis Today* **116**, 50–55.

Fauzia, S., Aziz, H., Dahlan, D. & Zein, R. 2018 Study of equilibrium, kinetic and thermodynamic for removal of Pb(II) in aqueous solution using Sago bark (Metroxylon sago). In: *AIP Conference Proceedings 2023*, p. 020081. https://doi.org/10.1063/1.5064078.

Freundlich, H. 1906 Over the adsorption in solution. *Journal of Physical Chemistry* **57**, 385–471.

Goncharuk, V. V., Kucheruk, D. D., Kochkodan, V. M. & Badekha, V. P. 2002 Removal of organic substances from aqueous solutions by reagent enhanced reverse osmosis. *Desalination* **143**, 45–51.

Han, S., Xu, J., Hou, W., Yu, X. & Wang, Y. 2004 Synthesis of high-quality MCM-48 mesoporous silica using Gemini surfactant dimethylene-1,2-bis (dodecyldimethylammonium bromide). *The Journal of Physical Chemistry A* **B108**, 15043–15048.

Hirakawa, T., Daimon, T., Kitazawa, M., Ohguri, N., Koga, C., Negishi, N., Matsuzawa, S. & Nosaka, Y. 2007 An approach to estimating photocatalytic activity of TiO_2 suspension by monitoring dissolved oxygen and superoxide ion on decomposing organic compounds. *Journal of Photochemistry and Photobiology A* **190**, 58–68.

Hu, H., Xu, K., 2020 Chapter 8 – physicochemical technologies for HRPs and risk control. In: *High-Risk Pollutants in Wastewater* (Ren, H. & Zhang, X. eds.). Elsevier, pp. 169–207. https://doi.org/10.1016/B978-0-12-816448-8.00008-3.

Humadi, J. I., Jafar, S. A., Ali, N. S., Ahmed, M. A., Mzeed, M. J., Al-Salhi, R. J., Saady, N. M. Cata, Majdi, H. Sh., Zendehboudi, S. & Albayati, T. M. 2023 Recovery of fuel from real waste oily sludge via a new eco-friendly surfactant material used in a digital baffle batch extraction unit. *Scientific Reports* **13**, 9931. https://doi.org/10.1038/s41598-023-37188-9.

Jabbar, N. M., Alardhi, S. M., Mohammed, A. K., Salih, I. K. & Albayati, T. M. 2022 Challenges in the implementation of bioremediation processes in petroleum-contaminated soils: A review. *Environmental Nanotechnology, Monitoring & Management* **18**, 100694. https://doi.org/10.1016/j.enmm.2022.100694.

Kadhum, S. T., Alkindi, G. Y. & Albayati, T. M. 2021 Determination of chemical oxygen demand for phenolic compounds from oil refinery wastewater implementing different methods. *Desalination and Water Treatment* **231**, 44–53. doi:10.5004/dwt.2021.27443.

Kadhum, S. T., Alkindi, G. Y. & Albayati, T. M. 2022 Remediation of phenolic wastewater implementing nano zerovalent iron as a granular third electrode in an electrochemical reactor. *International Journal of Environmental Science and Technology* **19**, 1383–1392. https://doi.org/10.1007/s13762-021-03205-5.

Khader, E. H., Khudhur, R. H., Abbood, N. S. & Albayati, T. M. 2023 Decolourisation of anionic azo dye in industrial wastewater using adsorption process: Investigating operating parameters. *Environmental Processes* **10**, 34. https://doi.org/10.1007/s40710-023-00646-7.

Khadim, A. T., Albayati, T. M. & Cata Saady, N. M. 2022 Removal of sulfur compounds from real diesel fuel employing the encapsulated mesoporous material adsorbent Co/MCM-41 in a fixed-bed column. *Microporous and Mesoporous Materials* **341**, 112020. https://doi.org/10.1016/j.micromeso.2022.112020.

Ko, C. H., Fan, C., Chiang, P. N., Wang, M. K. & Lin, K. C. 2007 *p*-Nitrophenol, phenol and aniline sorption by organo-clays. *Journal of Hazardous Materials* **149**, 275–282.

Koyuncu, H. & Kul, A. R. 2019 Removal of aniline from aqueous solution by activated kaolinite: Kinetic, equilibrium and thermodynamic studies. *Colloids and Surfaces A* **569**, 59–66.

Lagergren, S. 1898 About the theory of so-called adsorption of soluble substances. *Kungliga Svenska Vetenskapsakademiens. Handlingar* **24**(4), 1–39.

Levec, J. & Pintar, A. 2007 Catalytic wet-air oxidation processes: A review. *Catalysis Today* **124**, 172–184.

Liu, Q., Zhang, L., Hu, P. & Huang, R. 2015 Removal of aniline from aqueous solutions by activated carbon coated by chitosan. *Journal of Water Reuse and Desalination* **5**(4), 610–618. https://doi.org/10.2166/wrd.2015.097.

Morent, R., Dewulf, J., Steenhaut, N., Leys, C. & Van Lagenhove, H. 2006 Hybrid plasmacatalyst system for the removal of trichloroethylene from air. *Journal of Advanced Oxidation Technologies* **9**, 53–58.

Muslim, W. A., Albayati, T. M. & Al-Nasri, S. K. 2022 Decontamination of actual radioactive wastewater containing ^{137}cs using bentonite as a natural adsorbent: Equilibrium, kinetics, and thermodynamic studies. *Scientific Reports* **12**, 13837. https://doi.org/10.1038/s41598-022-18202-y.

Muslim, W. A., Al-Nasri, S. K. & Albayati, T. M. 2023 Evaluation of bentonite, attapulgite, and kaolinite as eco-friendly adsorbents in the treatment of real radioactive wastewater containing Cs-137. https://doi.org/10.1016/j.pnucene.2023.104730.

Narita, E., Horiguchi, N. & Okabe, T. 1985 Adsorption of phenols, cresols and benzyl alcohol from aqueous solution by silicalite. *Chemistry Letters* **6**, 787–790.

Nejat, R., Mahjoub, A. R., Hekmatian, Z. & Azadbakht, T. 2015 Pd-functionalized MCM-41 nanoporous silica as an efficient and reusable catalyst for promoting organic reactions. *RSC Advances* **5**, 16029–16035. 10.1039/C4RA11850B.

Pajchel, L. & Kolodziejski, W. 2018 Synthesis and characterization of MCM 48/hydroxyapatite composites for drug delivery: Ibuprofen incorporation, location and release studies. *Materials Science and Engineering C* **91**, 734–742. doi:10.1016/j.msec.2018.06.028.

Qiang, Z., Bao, X. & Ben, W. 2013 MCM-48 modified magnetic mesoporous nanocomposite as an attractive adsorbent for the removal of sulfamethazine from water. *Water Research* **47**, 4107–4114.

Saad, R., Belkacemi, K. & Hamoudi, S. 2007 Adsorption of phosphate and nitrate anions on ammonium-functionalized MCM-48: Effects of experimental conditions. *Journal of Colloid and Interface Science* **311**, 375–381.

Shaban, M., Abukhadra, M. R., Hamd, A., Amin, R. R. & Khalek, A. A. 2017 Photocatalytic removal of Congo red dye using MCM-48/Ni2O3 composite synthesized based on silica gel extracted from rice husk ash; fabrication and application. *Journal of Environmental Management* **204**, 189–199. doi:10.1016/j.jenvman.2017.08.048.

Taralkar, U. S., Kasture, M. W. & Joshi, P. N. 2008 Influence of synthesis condition on structure properties of MCM-48. *Journal of Physics and Chemistry of Solids* **69**(8), 2075–2081.

Temkin, M. & Pyzhev, V. 1940 Kinetics of ammonia synthesis on promoted iron catalyst. *Acta Physicochimica U.R.S.S.* **12**, 327–356.

Wang, X., Wang, Y., Shu, Z., Cao, Y., Wang, X., Zhou, F. & Huang, J. 2023 Phenolic hydroxyl-functionalized hyper-cross-linked polymers for efficient adsorptive removal of aniline. *Separation and Purification Technology* **305**, 122443. https://doi.org/10.1016/j.seppur.2022.122443.

Webber, T. & Chakkravorti, R. 1974 Pore and solid diffusion models for fixed-bed adsorbers. *American Institute of Chemical Engineers Journal* **20**, 228–238.

Yi, Z., Huajie, L., Mingchun, L. & Meihua, X. 2020 Adsorption of aniline on aminated chitosan/graphene oxide composite material. *Journal of Molecular Structure* **1209**, 127973. https://doi.org/10.1016/j.molstruc.2020.127973.

First received 9 May 2023; accepted in revised form 15 August 2023. Available online 30 August 2023